Polymer 51 (2010) 1737–1743

Contents lists available at ScienceDirect

Polymer

journal homepage: www.elsevier.com/locate/polymer

# *In-situ* QCM-D analysis reveals four distinct stages during vapour phase polymerisation of PEDOT thin films

Manrico Fabretto [a,b,*], Michael Müller [a], Colin Hall [a], Peter Murphy [b], Robert D. Short [b], Hans J. Griesser [a]

[a] Ian Wark Research Institute, University of South Australia, Mawson Lakes, SA 5095, Australia
[b] Mawson Institute, University of South Australia, Mawson Lakes, SA 5095, Australia

ARTICLE INFO

*Article history:*
Received 21 January 2010
Received in revised form
10 February 2010
Accepted 10 February 2010
Available online 16 February 2010

*Keywords:*
Poly(3,4-ethylenedioxythiophene) (PEDOT)
Vapour phase polymerisation (VPP)
Quartz crystal microbalance-dissipation (QCM-D)

ABSTRACT

Gaining a deeper understanding of the growth of poly(3,4-ethylenedioxythiophene) (PEDOT) films by vapour phase polymerisation (VPP) is essential for the rational design and optimization of such films. The VPP process was used to synthesise films of PEDOT on oxidant-coated substrates. Atomic force microscopy images showed that the morphology of the films changed considerably with time. Utilising a quartz crystal microbalance with dissipation measurement (QCM-D), we found that the kinetics of polymerisation and the viscoelastic properties of the films varied. The data reveal four distinct stages in film growth. Each stage produces a layer having different conductivity values, from a low of 276 S $cm^{-1}$ to a high of 1196 S $cm^{-1}$. Conductivity and electrochromic optical contrast, Δ%Tx, can thus be maximized by appropriate termination of the polymerisation reaction. Factors determining the polymerisation rate and changes in conductivity and optical performance are discussed.



## 1. Introduction

Over the past three decades, since the pioneering studies of Shirakawa and co-workers [1,2], advances in the field of inherently conducting polymers (ICPs) have furnished a plethora of organic electronic materials [3] that have been of interest for various applications such as actuators [4], organic thin-film transistors (OTFTs) [5], organic light emitting diodes (OLEDs) [6], organic photovoltaics (OPV) [7], supercapacitors [8,9], biosensors [10] and electrochromic devices [11,12]. Various ICPs have attracted intense interest and of these poly(3,4-ethylenedioxythiophene) (PEDOT) and its derivatives have arguably shown the greatest promise and versatility, with good chemical stability [13], high conductivity [14], and desirable electrochromic characteristics [15,16].

For most applications the conducting polymer needs to be deposited as a thin film onto a substrate; a ready means of achieving this is by spin- or spray-coating from an aqueous dispersion. Such dispersions, however, are known to form micelles with the polymer encapsulated in the insulating polyanion [17,18]. This creates ellipsoid molecular structures [19] resulting in a coating where the polymer does not attain a fully extended conformation, and this may ultimately affect the conductivity of the film [20]. Such a result may fall short of the required conductivity. The push for higher conductivity films has spawned the development of *in-situ* polymerisation, where the polymer is grown directly onto the substrate. Synthesis of conducting polymers in this manner has been achieved in three ways. One method is to spin a mixture of monomer, oxidant and inhibitor directly onto the substrate and as the inhibitor evaporates, synthesis is initiated [21]. The method is difficult to control as the ICP may form flocculants during the process, and great skill is required to obtain homogenous films [22]. Alternatively, electro-polymerisation [23,24] has been shown to produce acceptable ICP films. Two electrodes are inserted into a cell containing a solution of monomer and electrolyte, and a periodic voltage is cycled across the cell. Each cycle polymerises the monomer and simultaneously deposits the resultant polymer onto the substrate. A limitation of this method is that the polymer can only be formed on conducting substrates and film uniformity can be problematic for large depositions due to non-uniform electric fields. The third approach, which has gained acceptance and overcomes many of the drawbacks mentioned, is vapour phase polymerisation (VPP) [25–27]. An oxidant is deposited onto a substrate and acts as the polymerisation agent and, additionally, may also act as the dopant for the polymer. The substrate is placed into a chamber, a monomer vapour is introduced, and condensation of the monomer onto the substrate initiates the polymerisation process, creating a highly conducting film typically within 30 min.

* Corresponding author. Ian Wark Research Institute, University of South Australia, Mawson Lakes, SA 5095, Australia. Tel.: +61 8 8302 3675; fax: +61 8 8302 3683.
*E-mail address:* rick.fabretto@unisa.edu.au (M. Fabretto).

0032-3861/$ – see front matter © 2010 Elsevier Ltd. All rights reserved.
doi:10.1016/j.polymer.2010.02.019

The push towards utilising conducting polymers in various applications and devices has proceeded faster than the understanding of many fundamental issues that govern their growth during polymerisation. Mechanisms controlling the VPP process are complex and, to date, only partially understood. While the VPP process is essentially an interfacial growth phenomenon and ideally suited for measurement by the quartz crystal microbalance (QCM), there have been surprisingly few studies using the technique. Of these previous studies [28–32] most have focused on *in-situ* measurements of electrochemically synthesised conducting polymers, while even fewer studies [33–35] have utilised the technique for polymers synthesised using VPP.

Previous work [34] utilising the QCM demonstrated that the addition of a surfactant, whose primary function was to stop oxidant crystallisation, also delayed the onset of rapid growth during the VPP process. Using the conducting polymer PEDOT, the purpose of this study is to shed additional light on various aspects of the VPP process by utilising the QCM-D in conjunction with atomic force microscopy (AFM) time–evolution snapshots. The QCM-D technique has the ability to simultaneously measure the polymerisation rate and the viscoelastic property of the polymer during film formation. Results show that the VPP rate for PEDOT is far from linear and is in fact defined by four distinct stages which are accompanied by changes in the viscoelastic nature of the PEDOT film. These changes have an impact on the conductivity and electrochromic performance of the film. Accompanying AFM images are taken at various stages during the process and a mechanism controlling the polymerisation rate is proposed. Insights into this VPP process are likely to have general applicability, given the similar nature of oxidant-mediated vapour phase polymerisation of other ICPs.

## 2. Experimental section

Fe(III) tosylate was received from H. C. Starck as a 40 wt.% solution in butanol (Baytron CB 40). 3,4-Ethylenedioxythiophene (EDOT) monomer and poly(ethylene glycol-*ran*-propylene glycol) (PEG-*ran*-PPG), $M_w$ = 12 000 Da, were obtained from Aldrich. All chemicals were used without further purification.

Samples were prepared on glass substrates or indium tin oxide (ITO) glass cut into 5 × 5 cm plates. The substrates were washed using a mild detergent, followed by an ethanol and high purity water rinse. Substrates were further subjected to an air plasma treatment (PDC-32G, Harrick Inc.) for 2 min prior to coating. An oxidant solution consisting of 40 wt.% Baytron CB 40 and 60 wt.% *n*-butanol (*i.e.* 16 wt.% Fe(III) tosylate) was prepared, and to this 4 wt.% of PEG-*ran*-PPG was added. The solution was placed onto the substrates and spin-coated (400B-6NPP, Laurell Technologies Inc.) at a speed of 1000 RPM for 15 s. Samples were then placed on a hotplate set to 70 °C for 60 s to evaporate the butanol. Samples were removed from the hotplate and placed without delay into a 16 L glass polymerisation chamber (Fig. 1) and removed after a set time (ranging from 5 to 40 min). The chamber was operated at atmospheric pressure and placed on top of a hotplate set to 60–70 °C. This produced a temperature of 33 ± 1 °C on the surface of the substrate. The EDOT vapour concentration was kept in a state of saturation, as observed by condensation of the monomer on the chamber walls. Humidity and temperature inside the chamber were measured during the polymerisation process using a Sensirion Evaluation Kit (EK-H2, Sensirion) with an SHT15 sensor and an SF1 filter cap (Fig. 1). Relative humidity (RH) was set to 32 ± 2% throughout, with the addition of water drops (if necessary), after placing the samples into the chamber. During the polymerisation process, a magnetic stirrer bead was utilised at the bottom of the chamber for increased vapour circulation. Polymerisation kinetics were monitored using a quartz crystal microbalance (RQCM, Maxtek Inc.) coated with the oxidant solution and mounted close to the substrates within the chamber. At designated times the samples were removed from the polymerisation chamber and rinsed in an ethanol bath for 10 min to remove residual Fe(III) tosylate, dried with an air gun, followed by a final ethanol spray rinse and dried once more. Samples were then placed into an oven at 60 °C for 30 min to allow the film to cure. Post-rinsed samples were analysed using XPS to determine if any elemental iron remained in the film; within the resolution of the instrument no iron was detected.

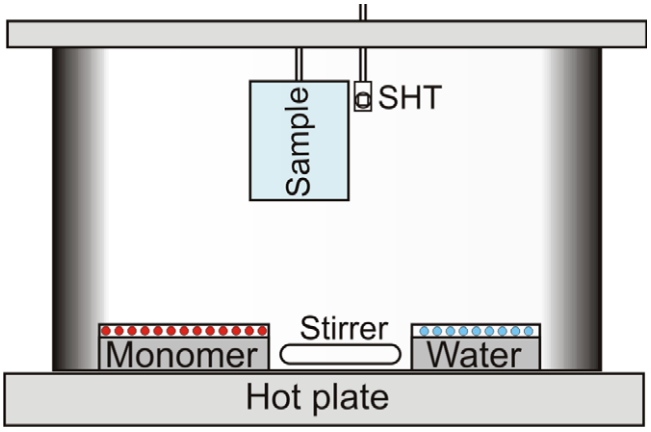


**Fig. 1.** Schematic diagram of the atmospheric VPP chamber. Oxidant-coated sample is suspended and a Sensirion humidity & temperature (SHT) sensor placed adjacent to the sample. Liquid EDOT monomer resides in a receptacle. Stirrer aids vapour dispersion. The VPP chamber resides on a hotplate; temperature in the range 60–70 °C.

Resistivity was measured using a four-point probe (RM3, Jandel Engineering), with 100 μm tip radius and 60 g preset load. Resistivity measurements were taken at room temperature (22 ± 2 °C) and humidity of 35 ± 5%, and are the average of at least nine measurements. Electrochromic activity was measured by placing the substrate into a cell and using a potentiostat (VoltaLab PGZ100, Radiometer Analytical) to switch the polymer between oxidized and reduced states. The cell was mounted within a spectrophotometer (UltraScan PRO, HunterLab Inc.), and percentage transmission changes were recorded. Values given are the photopic weighted average cantered at 555 nm using the CIE-1931 standard. AFM images and measurements (NTEGRA, NT-MDT) were performed in tapping mode. To calculate film thickness the polymer was carefully removed from sections of the substrate and the average of 10 line scans taken. Film thickness was then utilised together with the resistivity measurements to calculate the polymer's conductivity.

## 3. Results and discussion

### 3.1. Polymer film growth

Crystalline growth of VPP PEDOT has recently been reported [36] as well as crystallites of oxidant in other related work [37]. Our previous investigation [38] as well as this current study, however, found no evidence of any true crystalline PEDOT growth on any of the length scales investigated by AFM and SEM. Two of the most common oxidants used in VPP PEDOT are $FeCl_3$ and Fe(III) tosylate but their use is not without problems. Murphy and co-workers [38] demonstrated that crystallites formed in the oxidant under conditions of high humidity were due to the Fe(III) tosylate layer having an affinity for water absorption. The resulting VPP PEDOT film had numerous pinhole defects and a pseudo-crystalline appearance due to the suppression of polymerisation in the regions affected by the

crystallised oxidant. A surfactant (PEG-*ran*-PPG) was used to inhibit crystal formation, resulting in enhanced film formation and conductivity. Additionally, the surfactant also moderated the polymerisation rate which has prompted the more detailed investigation presented here.

The manner in which VPP PEDOT film formation occurs is the subject of much debate, and conjecture still exists as to whether film formation is a bottom up or top down process. Recently Nair et al. [39] suggested that PEDOT film formation occurred at the surface of the substrate, where the oxidant resided, and that polymer growth was a top down process. Once a skin layer had formed, additional polymer growth could only occur by accessing the oxidant via an EDOT diffusion process through the resulting PEDOT product layer. They reasoned that as film thickness increased, the process would become self-limiting due to the increasing difficulty in the diffusion of sufficient monomer through this layer. The results presented here, however, tend to support the notion that polymer growth is a bottom up process, and this concept will now be elucidated.

AFM images (Fig. 2; other length scales recorded but not shown) taken at various time intervals during the VPP process show that the morphology of the PEDOT layer evolves as the polymerisation

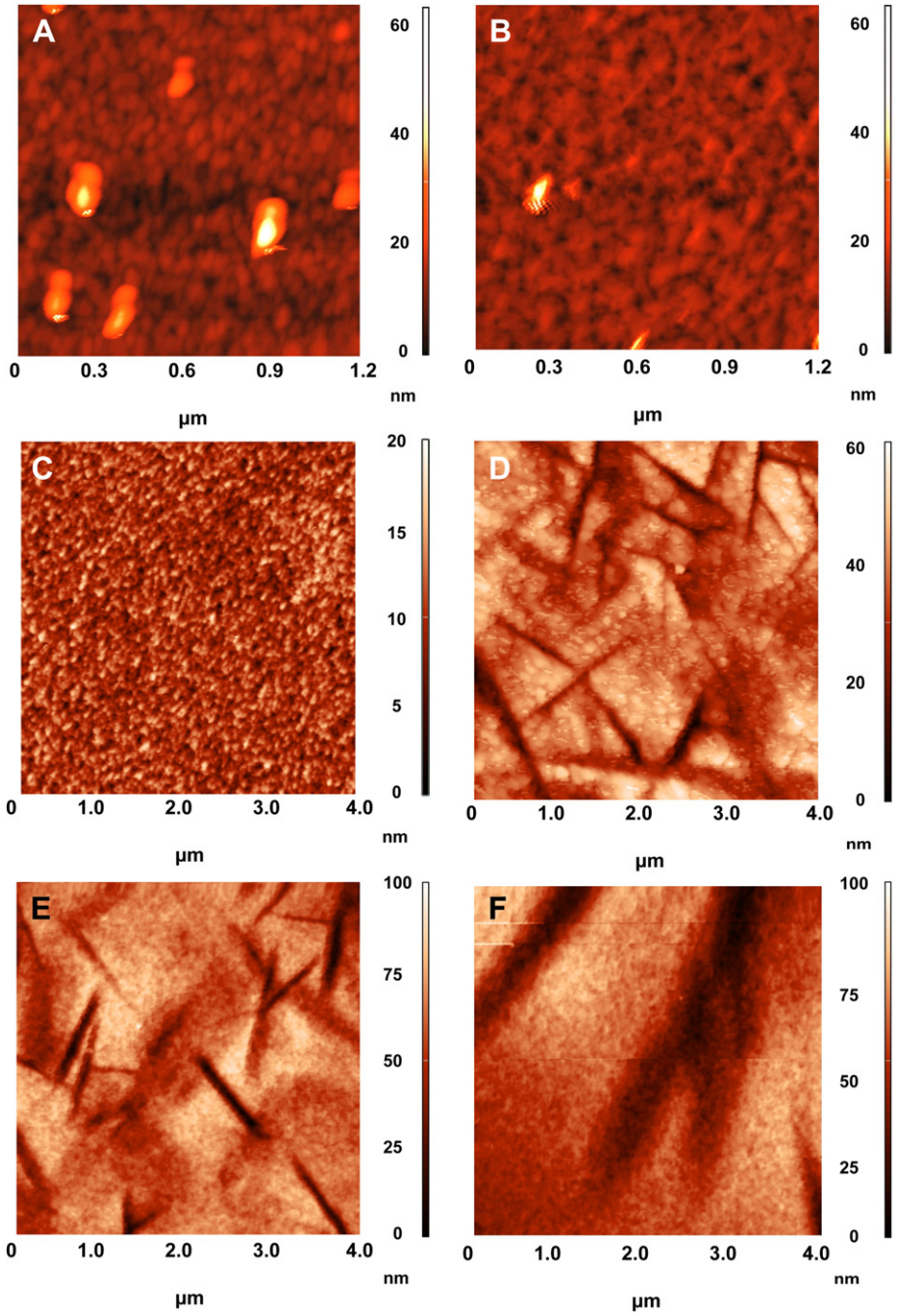


**Fig. 2.** AFM images of PEDOT film formation. A) 5 min: Formation of initial nodule layer, oxidant layer still visible (dark regions), bright spots indicate the formation of the second polymer layer. B) 10 min: Formation and interconnectivity of second layer, oxidant layer still visible. C) 15 min: Rapid formation of additional layers. D) 20 min: Polymer growth with fissures approx. 1 μm apart. E) 30 min and F) 40 min: Number of fissures decrease as preferential growth occurs along the fissure.

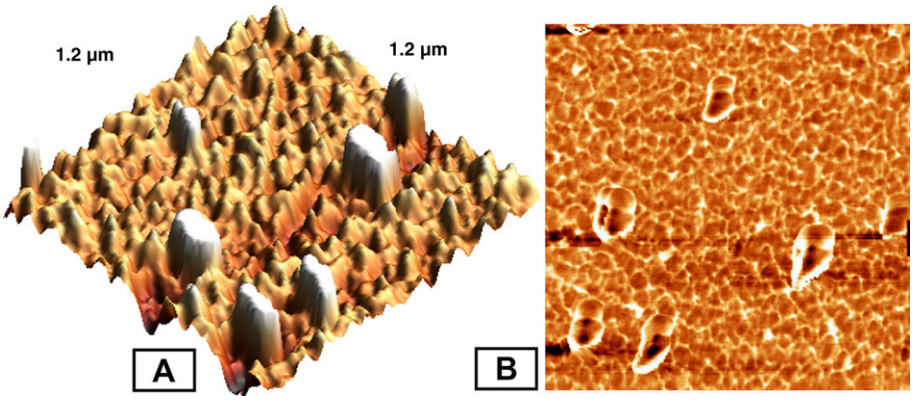


**Fig. 3.** A) 1.2 × 1.2 µm AFM 3D scan of PEDOT film formation after 5 min (same scan area as shown in Fig. 2A); B) phase image of the same.

progresses. Following nucleation, individual polymer nodules grow and eventually merge, followed by larger-scale morphological changes (to appreciate the significance of the images they are best viewed in conjunction with Fig. 4, which provides information on polymerisation rate and packing density during the process). In the first image (Fig. 2A) the VPP process was terminated after 5 min, and it shows the formation of distinct polymer nodules that form a loosely packed first layer. Additionally, the beginning of a second layer of polymer nodules is observed as indicated by the bright spots. The underlying oxidant, dark region (see also phase image Fig. 3B which clearly identifies the oxidant and nodular growth), is still clearly visible at this stage. Initial film formation appears to be the result of simultaneous nucleation and growth of many nodules, with the size of the nodules being of the order of 50 nm. Attempts to capture polymer film formation at an earlier stage proved problematic, with the PEDOT material delaminating during the washing process. This observation indicates that the adhesion of individual isolated polymer nodules to the substrate is not sufficiently strong to resist the forces applied during washing, and it is only after a percolation threshold has been reached that the cohesion of the film of interconnected nodules provides sufficient strength to avoid delamination. As growth continues, an additional layer begins to form on top of the initial layer but significant sections of oxidant-coated substrate are still visible, as shown in Fig. 2B: a strong indication that film growth is a bottom up process. At the 15 min mark (Fig. 2C) the loosely interconnected nodules have formed a tighter layer and virtually no oxidant is visible. Furthermore, figures (Fig. 2D–F) show fissures in the polymer surface being progressively filled. The alternate view that this is indeed crystal growth would appear to be inconsistent with the fact that the number of "crystals" decreases markedly from Fig. 2D to F. If this was indeed crystal growth, one would reasonably expect an increase in the size and number of crystals but this is clearly not the case. Thus, the time–evolution snapshots shown here strongly indicate that film growth is a bottom up process rather than a top down process and that fissures formed during polymer growth are preferentially backfilled as the process nears completion.

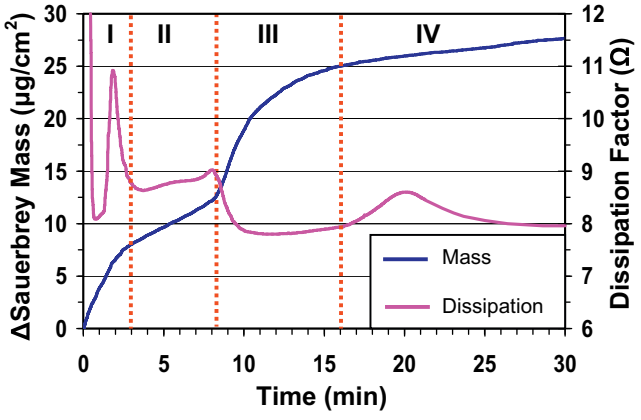


**Fig. 4.** Mass and dissipation measured by QCM-D during VPP of PEDOT at 60 °C. Four distinct growth rate stages (I–IV) are indicated with each producing a different conductivity value. The dissipation factor measures the viscoelastic properties of the polymer during polymerisation and is an indication of the change in packing density and/or conformation of the polymer.

The dissipation factor shown in Fig. 4 is a measure of the viscoelastic properties of an adsorbed layer [40–42], in our case this is a measure of packing density of the PEDOT film during formation. A rigidly attached layer will produce low dissipation, whereas a soft, loosely bound layer will cause the dissipation of the QCM-D system to increase due to increased dampening [43]. Examination of Fig. 4 shows that the dissipation factor was initially high and rapidly decreased in the first minute as polymer growth was initiated. The Fe(III) tosylate oxidant which is applied to the substrate is soft and tacky and so such an initial result is not unexpected. As polymer growth is established, the dissipation increases and this is consistent with the formation of small loosely bound nodules as indicated in Fig. 2A. This growth mechanism is further supported by the 3D and phase images in Fig. 3, which correspond to the same region scanned in Fig. 2A. As growth continues and the nodules begin to interconnect and form a continuous polymer film, they should start to behave as a more rigid body, and this is indeed evidenced by the decrease in dissipation at about the 3 min mark. The AFM images and dissipation data support the notion that polymer film formation, at least initially, occurs as distinct nodules that eventually merge to form a continuous network. The formation of a second nodular layer (Fig. 2B), prior to a complete first layer suggests that PEDOT seeding, once formed, has limited mobility. Fig. 3 shows AFM 3D and phase images of the PEDOT film at the 5 min mark. The 3D image shows distinct individual nodules (note that the *z*-axis scale is in nm compared to *xy*-axis which is in µm) with the phase imaging supporting the notion that in the early polymerisation stages the small nodules are separated by the underlying oxidant. Subsequent statistical analysis of the height distribution on the surface of the substrate (5 min mark) generated a large positive kurtosis number (kurtosis = +18), an indication that the height distribution was very narrow (a kurtosis number of zero indicates a Gaussian height distribution). Such a high kurtosis number is consistent with initial seeding followed by nodular growth with little or no growth recorded in-between. After the initial seeding phase, as

polymerisation continued, the kurtosis number decreased markedly (to a value of +0.6) for the latter samples (Fig. 2B–F, 10–40 min), which is an indication that the height distribution (growth) is Gaussian. Our interpretation is that after the initial seeding phase, additional growth occurs in a random manner and assumes a Gaussian probability distribution. Fig. 2B shows the formation of a second layer with some loosely interconnected nodules present, which is supported by the slowly increasing dissipation factor from the 3 to 8 min mark as shown in Fig. 4. Areas of oxidant-coated substrate are still visible and film growth during stage II slowed (compared to stage I). Given that the relative humidity was maintained at a constant 32 ± 2% and that the monomer vapour remained saturated, the reduced growth rate can be explained in terms of a drop in the apparent oxidant reactivity. This concept will now be examined in greater detail.

Fig. 5 shows two polymerisation curves, one run at 60 °C, the other at 70 °C (hotplate temperatures in the range 40–80 °C were tried and produced only small changes in substrate temperature ≲2 °C). Too low a hotplate temperature resulted in poor reproducibility as changing ambient conditions influenced the VPP process. Too high a hotplate temperature also resulted in poor film formation. Additionally, it was found necessary to pre-heat the substrates to 30–32 °C prior to placement in the chamber. Placing ambient temperature substrates into the chamber resulted in condensation and macroscopic droplets forming on the plates with subsequent poor film formation. Conversely, too high a substrate temperature produced no condensation, resulting in delayed film formation until the substrate cooled.

Initially, the rate-limiting step in film growth is governed by the amount of monomer and/or water vapour transported to the oxidant-coated substrate. An increase in hotplate temperature increases the vapour pressure of the monomer and water and hence the transportation rate to the substrate surface. The arrival rate of monomer and water vapour to the substrate surface dictates the rate of polymer film growth, as the amount of oxidant available can be considered infinite. The increase in polymerisation rate shown in Fig. 5 is clearly seen in stage I and the early part of stage III. As film growth progresses, the availability of exposed oxidant diminishes and a new growth regime occurs when the coverage approaches a confluent layer of polymer nodules (stage II). Since film formation is based on an oxidative first step [44], the formation of additional layers still requires the removal of an electron from the monomer to initiate polymerisation. Electron acceptance by the oxidant, however, must now occur through a conductive pathway (*i.e.* the initial PEDOT layer), rather than directly from monomer to oxidant. Oxidation of the monomer via electron transfer must now proceed through the initially formed PEDOT layer, and the efficiency of this process dictates the rate of polymerisation during this stage. The reduced polymerisation rate can be explained in terms of percolation theory, where the initial number of interconnecting PEDOT pathways having the ability to transport electrons to active oxidant sites is small. Limited transportation pathways to active oxidant sites is now the rate-limiting step in the polymerisation process. This phenomenon, if correct, would produce the same effect as would a real change in the reactivity of the oxidant. As the VPP process continues, the polymer nodules form a confluent layer and polymer growth once again accelerates and becomes similar to that in stage I. This observation can be rationalized in terms of the confluent layer of polymer nodules possessing better access to the active oxidant centres compared to a system where the interconnectivity of the nodules resides below the percolation threshold. Thus, once the percolation threshold is achieved, multiple electron conduction pathways between the surface layer and the oxidant enable efficient electron transfer. Hence the rate-limiting step, once again, becomes the arrival rate of the monomer and/or water vapour onto the surface of the substrate. If film formation was a top down process governed by diffusion of the monomer to the oxidant surface through the PEDOT film, as suggested by Nair et al. [39], then the increased polymerisation rate noted in stage III would not occur. The more plausible explanation is thus a bottom up film formation.

Interestingly, the onset of rapid polymer growth produces a decrease in the dissipation factor, indicating that the packing density increases. Conductivity data (Table 1), however, indicate that the conductivity during this stage is relatively poor. Given that the packing density is higher but conductivity is lower, a plausible explanation is that the polymer chains formed during this period may contain an increased number of defects. This is supported by an earlier work [45] which showed a decrease in doping levels under less than optimum polymerisation conditions. Finally, as the oxidant is consumed in the process and availability diminishes, film growth once again slows and the dissipation slowly increases, indicating formation of a looser top layer (Fig. 2; 15–20 min). The dissipation factor, however, starts to decrease from about the 20 min mark, indicating an increase in packing density. This is supported by the AFM images (Fig. 2D–F) that show large fissures slowly closing up with new growth, and indicate that preferential growth occurs along the fissures as the last of the oxidant is consumed.

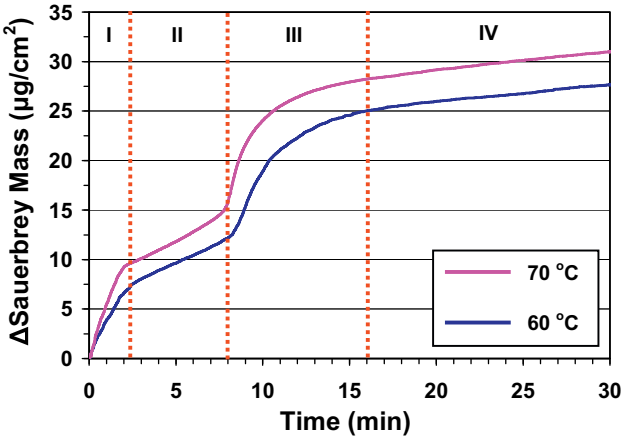


**Fig. 5.** Change in Sauerbrey Mass vs. time measured using QCM-D, for PEDOT films grown at hotplate settings of 60 °C and 70 °C, respectively. Shown are the four distinct growth stages I–IV.

### 3.2. Polymer conductivity

Of special interest is the fact that the conductivity of the films terminated at different polymerisation times is not constant but varies during polymer growth and depends upon when the process

**Table 1**
Overall film conductivity and estimated conductivity of sectional layers required to produce the observed overall conductivity values, assuming a multi-layer structure, for VPP PEDOT films at various processing times.

| Measurement taken at: | Overall film conductivity (S cm$^{-1}$) | Section conductivity (S cm$^{-1}$) |
|---|---|---|
| End of stage I | 867 | 867 |
| Mid-point of stage II | 974 | 1098 |
| End of stage II | 1078 | 1196 |
| End of stage III | 723 | 428 |
| Mid-point of stage IV | 635 | 276 |
| End of stage IV | 669 | 402[a] |

[a] Film thickness at the end of stage IV was slightly less than at mid-point of stage IV, indicating that the film had undergone some form of compaction.

was terminated. Table 1 indicates that the initial overall conductivity in stage I is high, 867 S cm$^{-1}$, and further increases in the early stages, with a maximum conductivity of 1078 S cm$^{-1}$ recorded at the end of stage II. This trend was consistent over a number of individual polymerisation runs. At the end of stage III the overall conductivity dropped to 723 S cm$^{-1}$ and continues to decrease to a value of 635 S cm$^{-1}$ by the mid-point of stage IV. At the end of stage IV the conductivity has increased slightly to 669 S cm$^{-1}$. Note that the error in the conductivity values presented is less than ±10% relative (established over several polymerisation runs). Repeated polymerisation runs typically produced small increases in film thickness during the last part of stage IV, but on occasions a small decrease was actually recorded. Such results tend to indicate a degree of film rearrangement and/or compaction during the last stages of synthesis and this phenomenon produces the slight increase in conductivity, rather than any intrinsic increase in the conductivity of the film in the latter stages. This notion is further supported by the drop in dissipation after the 20 min mark, as shown in Fig. 4. Since the overall conductivity is the additive of each (sectional) stage, taking into account the new film thickness, the changes in sectional conductivity for each layer are significant and these are presented in the last column of Table 1. A peak value of 1196 S cm$^{-1}$ is recorded for the growth obtained from the mid-point of stage II to the end of stage II. These results indicate that films with maximum conductivity are produced when the polymerisation rate is at its slowest due, in part, to the higher degree of order and alignment that are afforded by a slow polymerisation rate. Not unexpected then is the fact that a significant decrease in conductivity is noted during stage III, when polymer growth rate is at its highest. The sustained poor conductivity in the last stage, accompanied by a reduction in the rate of polymer growth, can be attributed to the amount of oxidant now remaining being below the level necessary for continuous undisrupted film growth. This concept is supported by previous work [34,45] which showed a drop in PEDOT film doping levels under less than favourable polymerisation conditions.

### 3.3. Optical transmission/electrochromic switching

Evaluating conducting polymers typically involves measuring the conductivity and/or the optical characteristics, including electrochromic switching of the material. In general, researchers have not measured the two characteristics concurrently to establish whether their performance is linked in some manner. Two samples, one terminated at the end of stage II (high conductivity) and the other at the end of stage IV (low conductivity), were evaluated for optical transmission properties. Both films were mounted into an optical cell containing an ionic liquid electrolyte and the potential switched between −700 mV and +1100 mV to reduce and oxidize the polymer. The results are shown in Fig. 6. The high conductivity polymer sample showed superior optical performance, with the photopically averaged (centred at 555 nm) optical contrast having a switching range of Δ%Tx = 46.1% compared with that of the lower conductivity sample, which measured Δ%Tx = 42.3%. Interestingly, the improvement in the optical switching range is a consequence of increased attenuation primarily in the reduced state (darkened) rather than increased transmission in the oxidized state (bleached).

The link between disrupted conjugation due to defects along the polymer backbone and a decrease in conductivity is well established [46–48]. Given this fact, how does one reconcile the phenomenon of increased optical range being a consequence of increased optical attenuation in the reduced state only (with minimal optical difference in the oxidized state)? We propose that conjugation defects along the polymer backbone lead to small

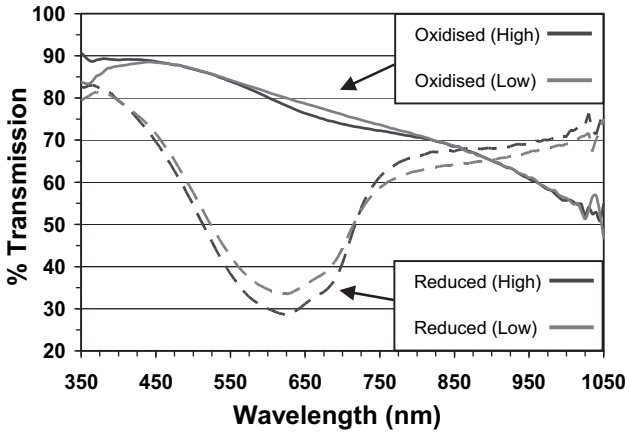


**Fig. 6.** Electrochromic activity in reduced and oxidized states for PEDOT samples produced with polymerisation times of ≈10 min (high conductivity) and ≈30 min (low conductivity). Note that the increased electrochromic %transmission range is a result of increased attenuation in the darkened state. (Note: Film thickness has been normalized to 70 nm for both samples).

segments or pockets that are inaccessible to electronic charge ingress/egress. During polymer synthesis, however, dopant counterions still migrate into these regions largely unaffected by point defects along the polymer. Other studies [49,50] have used XPS to measure PSS$^{(-)}$ and tosylate$^{(-)}$ doping levels, and this study has likewise utilised XPS to measure the tosylate$^{(-)}$ doping levels present in the PEDOT polymer. The XPS S(2p) signal is well suited to this measurement and high resolution analysis easily separates the contributions from the S(2p) moiety associated with the thiophene ring (PEDOT) and from the sulfonate S(2p) moiety associated with the tosylate$^{(-)}$ counterion. Our XPS S(2p) spectra were very similar in general appearance to those of an earlier study by Zotti et al. [49] (and have been reported elsewhere [34,45]). Importantly, however, variations in the doping level were recorded through the various PEDOT layers. For PEDOT produced up to the end of stage II the doping ratio was consistently in the range 1:3.7–4.0 (*i.e.* one tosylate counterion for approximately every four PEDOT repeat units) for the various samples examined in this study. Additionally, PEDOT films were peeled away from their substrates and the backside of the PEDOT film was analysed. Since XPS is a surface sensitive measurement, analysis of the backside of the film enabled the doping levels produced during the early part of stage I to be recorded. Stage I consistently gave a doping ratio of 1:4.0. In comparison, the doping ratio recorded in stage IV reduced to 1:4.6. It is difficult to definitively state whether changes in conductivity and electrochromic switch are due to differences in chemical composition (doping levels) or packing density and microstructure, as the data indicate that both occur during the polymerisation process. Close examination of the dissipation curve in Fig. 4 and the conductivity recorded in Table 1 indicates that conductivity increased in the transition from stages I to II and decreased in the transition from stages II to III. The dissipation factor, however, decreased on both occasions. As such, assigning packing density and microstructure as the dominant cause for changes in conductivity would be inconsistent. The level of doping, however, increased from stages I to II and decreased from stages II to IV and such a result is consistent with the changes in conductivity that were recorded. Thus, the observed differences in conductivity and electrochromic switching are most likely due to differences in the doping levels during polymerisation. Given the fact that there is sufficient oxidant available up to the end of stage III, a drop in doping levels is consistent with the fact that conjugation along the polymer backbone is compromised in some manner during

stage III. This is most likely the result of defects along the conjugated backbone, and this gives rise to a lower doping level.

Thus it appears reasonable to postulate that point defects resulting in discontinuous conjugation, rather than micro-structural factors such as packing density, play the most important role in the performance of VPP PEDOT films. Furthermore, a correlation between fast polymerisation rate and poorer conductivity (*i.e.* during stage III) appears to be evident. The results support the notion that poor quality PEDOT has conductively isolated pockets of polymer that become locked in an oxidized state during synthesis. These isolated regions are unable to support electronic charge ingress/egress and thus do not participate in effective redox activity. In contrast, high conductivity PEDOT films have fewer defects along the polymer backbone, leading to a situation where a greater proportion of the polymer can be fully reduced, thus increasing the electrochromic switching range. This interpretation is consistent with the observed increase in the optical range occurring as a consequence of increased attenuation in the reduced state.

## 4. Conclusions

The kinetics of PEDOT polymer synthesis using vapour stage polymerisation have been investigated. For the first time, AFM images have captured the evolution of PEDOT film structure together with concomitant QCM-D data; the observations reveal four distinct growth stages. The conductivity of the PEDOT film in each growth stage is different and kinetic results obtained via QCM-D indicate that the best conductivity (1078 S $cm^{-1}$) and largest electro-optical switching range ($\Delta$%Tx = 46.1%) are obtained when polymer synthesis is terminated prior to undergoing rapid growth (beginning of stage III). Allowing the process to continue into stage III results in decreased conductivity and electrochromic performance. Reduced doping levels post-stage III point to the most likely cause being disrupted conjugation along the polymer backbone rather than changes in the polymer's packing density. Understanding of the growth mechanism and its impact on conductivity and electrochromic switching is an essential aspect of future work, with the rational design and implementation of a better VPP process likely to lead to enhanced PEDOT performance.

## Acknowledgements

The authors acknowledge financial support by the Australian Commonwealth Government (ARC Linkage grant LP0668876) and thank Dr. A. Michelmore for AFM and XPS analysis.

## References

[1] Chiang C, Fincher C, Park Y, Heeger AJ, Shirakawa H, Louis E, et al. Phys Rev Lett 1977;39(17):1098–101.
[2] Shirakawa H, Louis E, MacDiarmid AG, Chiang C, Heeger AJ. J Chem Soc, Chem Commun 1977;474:578–80.
[3] Angelopoulos M. IBM J Res Dev 2001;45(1):57–75.
[4] Spinks G, Xi B, Zhou D, Truong V-T, Wallace GG. Synth Met 2004;140(2–3):273–80.
[5] Backlund T, Sandberg H, Osterbacka R, Stubb H, Makela T, Jussila S. Synth Met 2005;148:87–91.
[6] de Cuendias A, Urien M, Lecommandoux S, Wantz G, Cloutet E, Cramail H. Org Electron 2006;7:576–85.
[7] Ryuzaki S, Onoe J. J Appl Phys 2009;106:0235261–5.
[8] Vaillant J, Lira-Cantu M, Cuentas-Gallegos K, Casan-Pastor N, Gomez-Romero P. Prog Solid State Chem 2006;34:147–59.
[9] Ryu K, Lee Y-G, Hong Y-S, Park Y, Wu X, Kim K, et al. Electrochim Acta 2004;50:843–7.
[10] Kros A, Nolte R, Sommerdijk N. J Polym Sci Part A: Polym Chem 2002;40:738–47.
[11] Welsh DM, Kumar A, Meijer EW, Reynolds JR. Adv Mater 1999;11(16):1379–82.
[12] Bhandari S, Deepa M, Srivastava A, Joshi A, Kany R. J Phys Chem B 2009;113:9416–28.
[13] Winther-Jensen B, West K. React Funct Polym 2006;66:479–83.
[14] Fabretto M, Zuber K, Hall C, Murphy P. Macromol Rapid Commun 2008;29:1403–9.
[15] Gaupp CL, Welsh DM, Reynolds JR. Macromol Rapid Commun 2002;23(15):885–9.
[16] Reeves BD, Grenier CRG, Argun AA, Cirpan A, McCarley TD, Reynolds JR. Macromolecules 2004;37:7559–69.
[17] Nardes A, Kemerink M, Janssen R, Bastiaansen J, Kiggen N, Langeveld B, et al. Adv Mater 2007;19:1196–200.
[18] Ionescu-Zanetti C, Mechler A, Carter S, Lal R. Adv Mater 2004;16(5):385–9.
[19] Timpanaro S, Kemerink M, Touwslager FJ, De Kok MM, Schrader S. Chem Phys Lett; 2004:339–43.
[20] Fabretto M, Hall C, Vaithianathan T, Innis P, Mazurkiewicz J, Wallace GG, et al. Thin Solid Films 2008;516:7828–35.
[21] Pettersson L, Carlsson F, Inganas O, Arwin H. Thin Solid Films 1998;313–314:356–61.
[22] Winther-Jensen B, West K. Macromolecules 2004;37:4538–43.
[23] Groenendaal L, Zotti G, Jonas F. Synth Met 2001;118:105–9.
[24] Cho S, Xiao R, Lee S. Nanotechnology 2007;18:1–5.
[25] Kim J, Kim E, Won Y, Lee H, Suh K. Synth Met 2003;139:485–9.
[26] Lock J, Im S, Gleason K. Macromolecules 2006;39:5326–9.
[27] Winther-Jensen B, Breiby DW, West K. Synth Met 2005;152:1–4.
[28] Bailey L, Kambhampati D, Kanazawa KK, Knoll W, Frank C. Langmuir 2002;18:479–89.
[29] Schweiss R, Lubben J, Johannsmann D, Knoll W. Electrochim Acta 2005;50:2849–56.
[30] Bund A, Baba A, Berg S, Johannsmann D, Lubben J, Wang ZY, et al. J Phys Chem B 2003;107:6743–7.
[31] Lassalle N, Roget A, Livache T, Mailley P, Vieil E. Talanta 2001;55:993–1004.
[32] Wudy F, Schedlbauer T, Stock C, Gores H. Acta Chim Slov 2009;56(1):65–9.
[33] Nair S, Natarajan S, Kim S. Macromol Rapid Commun 2005;26:1599–603.
[34] Fabretto M, Muller M, Zuber K, Murphy P. Macromol Rapid Commun 2009;30:1846–51.
[35] Winther-Jensen B, Chen J, West K, Wallace GG. Macromolecules 2004;37:5930–5.
[36] Kim J-Y, Kwon M-H, Min Y-K, Kwon S, Ihm D-W. Adv Mater 2007;19(21):3501–6.
[37] Chen J, Winther-Jensen B, Pornputtkul Y, West K, Kane-Maquarie L, Wallace GG. Electrochem Solid State Lett 2006;9(1):C9–11.
[38] Zuber K, Fabretto M, Hall C, Murphy P. Macromol Rapid Commun 2008;29:1503–8.
[39] Nair S, Hsiao E, Kim S. Chem Mater 2009;21:115–21.
[40] Buttry D, Ward M. Chem Rev 1992;92(6):1355–79.
[41] Notley S, Eriksson M, Wagberg L. J Colloid Interface Sci 2005;292:29–37.
[42] Wagberg L, Pettersson G, Notley S. J Colloid Interface Sci 2004;274:480–8.
[43] Hook F, Rodahl M, Brzezinski P, Kasemo B. J Colloid Interface Sci 1998;208:63–7.
[44] Ha Y-H, Nikolov N, Pollack SK, Mastrangelo J, Martin BD, Shashidhar R. Adv Funct Mater 2004;14(6):615–22.
[45] Fabretto M, Zuber K, Hall C, Murphy P, Griesser H. J Mater Chem 2009;19:7871–8.
[46] Carrasco P, Grande H, Cortazar M, Alberdi J, Areizaga J, Pomposo J. Synth Met 2006;156:420–5.
[47] Chang Y-M, Su W-F, Wang L. Sol Energy Mater 2008;92:761–5.
[48] Marciniak S, Crispin X, Uvdal K, Trzcinski M, Birgerson J, Groenendaal L, et al. Synth Met 2004;141:67–73.
[49] Zotti G, Zecchin S, Schiavon G, Louwet F, Groenendaal L, Crispin X, et al. Macromolecules 2003;36:3337–44.
[50] Kim TY, Park CM, Kim JE, Suh KS. Synth Met 2005;149:169–74.